
**Aerosol Science and Technology**
Publication details, including instructions for authors and subscription information:
http://www.informaworld.com/smpp/title~content=t713656376

# Light Scattering Study of Aggregation Kinetics in Dense, Gelling Aerosols

R. Dhaubhadel [a]; A. Chakrabarti [a];C. M. Sorensen [a]
[a] Department of Physics, Kansas State University, Manhattan, Kansas, USA

First published on: 01 November 2009

**To cite this Article** Dhaubhadel, R. , Chakrabarti, A. andSorensen, C. M.(2009) 'Light Scattering Study of Aggregation Kinetics in Dense, Gelling Aerosols', Aerosol Science and Technology, 43: 11, 1053 — 1063, First published on: 01 November 2009 (iFirst)
**To link to this Article: DOI:** 10.1080/02786820903136908
**URL:** http://dx.doi.org/10.1080/02786820903136908

*Aerosol Science and Technology*, 43:1053–1063, 2009

ISSN: 0278-6826 print / 1521-7388 online
DOI: 10.1080/02786820903136908

# Light Scattering Study of Aggregation Kinetics in Dense, Gelling Aerosols

**R. Dhaubhadel, A. Chakrabarti, and C. M. Sorensen**
*Department of Physics, Kansas State University, Manhattan, Kansas, USA*



**We report the results of a study of the kinetics of a dense aggregating aerosol system that show that the predictions of the Diffusion Limited Cluster Aggregation (DLCA) model no longer hold when the system is dense. We studied a soot aerosol using the small angle light scattering technique created by exploding a mixture of a hydrocarbon gas and oxygen in a closed chamber. The soot particles started as individual monomers, ca. 38 nm radius, grew to bigger fractal clusters with time and finally stopped evolving after spanning a network across the whole system volume. This spanning is aerosol gelation. The study of the kinetics of the aggregating system showed that as the system evolved from a cluster dilute to cluster dense system, the aggregation kernel homogeneity λ evolved from the dilute limit, DLCA value of zero to a value 0.42 +/− 0.05 at the gel point. This evolution is consistent with previous simulation and theory. The experimental value at the gel point is nearly equal to the value of 0.5 predicted by simulation and theory. In addition, the magnitude of the aggregation kernel showed an increase with increasing volume fraction.**

## INTRODUCTION

Aggregation of particles in aerosols and colloids is a very important phenomenon in physics, biology, and material science (Family and Landau 1984; Jullien and Botet 1987; Meakin 1988; Friendlander 2000). Brownian motion, fluid shear and differential settling, can all cause aggregation. By controlling the particle interaction it is possible to aggregate non-coalescing particles with a variety of microstructures (Chakrabarti et al. 2004) ranging from ordered two-dimensional and three-dimensional nanocrystal superlattices (Murray et al. 1995; Lin et al. 2001), to fractal-like aggregates and gelled, percolated network structures (Meakin 1999; Seaton and Glandt 1987). A deep understanding of the structure of particle aggregates and the kinetics of their formation is the key to explain and control many complex but important phenomena in many different fields including material and biomedical science and industry.

In this work we continue our studies of aggregation and gelation in dense aerosols (Sorensen et al. 1998; Sorensen and Hageman 2001; Sorensen et al. 2003; Fry et al. 2002, 2004; Kim et al. 2004, 2006; Dhaubhadel et al. 2006, 2007). Here we study the aggregation kinetics of a cloud of smoke that gelled on the order of 100 seconds after its creation. Our description requires some new definitions. We will describe a system as dilute when the average cluster-cluster separation is very large compared to the cluster size, and we will call this situation *cluster dilute*. Then the average cluster-cluster separation is not a relevant length scale. Such aggregation has been well represented by the diffusion limited cluster-cluster aggregation (DLCA) model (Meakin 1983; Kolb and Jullien 1983). However, in a fractal aggregation process, for which the fractal dimension $D_f$ is less than the spatial dimension $d$, the growth kinetics causes the aggregates to occupy a increasing fraction of the available space with time. The average cluster-cluster separation then no longer remains large compare to the cluster size. We define such situation as *cluster dense*. Cluster dense aerosols may be found in practical situations in industry such as the synthesis of carbon black.

Smoluchowski's coagulation rate equation (SE) can well describe the aggregation kinetics of non-equilibrium systems in the cluster dilute limit (Friedlander 2000; Smoluchowski 1917). The SE is based on a mean-field theory which can predict system behaviours only in the limit of spatially uncorrelated binary cluster collisions. Systems with low particle concentration are in this limit. For a continuous cluster size distribution with cluster number density $n(v, t)$ of size $v$ (mass or monomer number) at time $t$, the SE is given as,

$$\frac{\partial n(v,t)}{\partial t} = \frac{1}{2}\int_0^v K(v-u,u)n(v-u,t)n(u,t)du - n(v,t)\int_0^\infty K(v,u)n(u,t)du. \quad [1]$$

The first term on the r.h.s. of this equation describes the gain while the second term the loss of clusters of size $v$ at time $t$ during the collision and sticking process of the clusters. Also

Received 9 March 2009; accepted 21 April 2009.
This work was supported by the NASA grant NNC04GA74G and a grant from the Cabot Corporation.
Address correspondence to C. M. Sorensen, Department of Physics, Kansas State University, Manhattan, Kansas, 66506-2601, USA. E-mail: sor@phys.ksu.edu

$K(v, u)$ is the aggregation kernel which describes the rate of clustering between particles of size $v$ and size $u$. The SE can be solved analytically when the kernel is a homogeneous function (Friedlander 2000),

$$K(cv, cu) = c^{\lambda} K(v, u) \quad [2]$$

where $\lambda$ is the kernel homogeneity relevant for many physical situations. The kernel depends on the collision interaction among the clusters, viz., sticking probability of particles upon collision, type of particle motion (diffusive, shear flow, gravitational settling, etc.), sizes of the interacting particles, and so on.

For a cluster dilute system where particles undergo Brownian diffusional motion, the aggregation process, based on the sticking probability ($p$), is either diffusion limited cluster aggregation (DLCA) when $p = 1$, or reaction limited cluster aggregation (RLCA) when $p \ll 1$ (Vicsek 1989; Meakin 1992). Both DLCA and RLCA processes lead to the formation of fractal structures whose density decreases as the number of monomers in aggregate increases. This property of a fractal aggregate is a consequence of its fractal dimension $D_f$ which is less than the spatial dimensional $d$. The number of monomers $N$ (equivalent to $v$ and $u$ above) contained by a fractal aggregate with radius of gyration $R_g$ is given by a simple fractal scaling law as

$$N = k_0 \left(R_g/a\right)^{D_f}. \quad [3]$$

Here the prefactor $k_0 \approx 1.3$ for DLCA (Sorensen and Roberts 1997; Cai et al. 1995) and $a$ is the monomer size (radius). The fractal morphology of DLCA aggregates in the dilute limit is now well established as having a mass fractal dimension of $D_f \approx 1.8$ (Family and Landau 1984; Jullien and Botet 1987; Meakin 1988).

The study of cluster dense systems is relatively new. A few simulations (Gimel et al. 1995; Kolb and Herrmann 1985; Hasmy and Jullien 1996; Rottereau et al. 2004; Fry et al. 2002; Fry et al. 2004; Heine et al. 2006; Heine and Pratsinis 2007) and a few experimental studies (Sorensen et al. 2003; Kim et al. 2004; Dhaubhadel et al. 2006; Kim et al. 2006) are found in the literature that study aggregation from the dilute regime up to the cluster dense regime. Previous simulation studies of aggregation were limited in time and/or system size (however, see below) with smaller volume fractions so that the cluster dense regime was not attained. Also most of the previous experimental attempts were limited to smaller monomer volume fractions such that the time the system would have taken to cross over from cluster dilute to cluster dense was much longer than the typical experimental observation time.

Our previous large-scale computer simulations of cluster-cluster aggregation (Fry et al. 2003, 2004) have shown that the cluster motion evolved from Brownian diffusion (DLCA) to ballistic motion as the system crossed over from the cluster dilute to the cluster dense regime. We found that the kinetic exponent $z$ in the power-law cluster radius of gyration growth with time $t$, i.e. $R_g \sim t^{z/D_f}$, continuously evolved from 1 to 2, and the aggregation kernel homogeneity $\lambda$ concomitantly (see Equation [15]) evolved from 0 to 0.5. The kinetic exponent $z = 1$ and the homogeneity $\lambda = 0$ during the early dilute stage of the aggregation process were as expected for DLCA. The observed $z = 2$ and $\lambda = 0.5$ in the dense regime implied a ballistic-type aggregation. In this late stage process the aggregating clusters move along the short straight paths between successive collisions with speed determined by the equipartition of energy. Both parameters $z$ and $\lambda$ were found to be universal functions of the free volume $\Omega$, which is the volume not occupied by the growing clusters. The cluster crowding is found to be the only reason for the enhanced aggregation kinetics.

Gimel et al. (1995) and Rottereau et al. (2004) recognized the crossover process to be explainable by static percolation theory. From their extensive computer simulation study, they found that systems undergoing the DLCA process eventually become cluster dense and finally gel irrespective to their monomer volume fraction provided the system size tends to infinity. This crossover from dilute to dense occurs at a characteristic size which is determined by the overlap of the clusters and decreases with increasing monomer volume fraction. Also the sol-gel transition occurs at a well-defined time. They observed strong modifications in both the cluster size distribution and the mass fractal dimension as the aggregation process crosses over from cluster dilute regime to cluster dense regime. In their simulation studies, Gimel et al. (1995) used the mean field Smoluchowski Equation (SE) approach to describe the cluster aggregation kinetics in the early dilute state, but the connectivity network of the fractals during the gelation of the system was explained in terms of the percolation theory. The DLCA and percolation clusters are characterized by the scaling size distribution exponents of 0 and 2.18, respectively. They found that the morphology of the space filling network of clusters is the same whether it is a result of a dynamic DLCA process or a static percolation process. They also observed a transition in the fractal dimension from that expected for DLCA to that expected for percolation. They found dilute limit DLCA fractal dimension of 1.8 at smaller length scales and percolating cluster fractal dimension of 2.5 at larger length scales. All these results are consistent with our simulation results.

Other simulation studies on dense systems have found a fractal dimension intermediate between that for DLCA clusters and percolation clusters (Kolb and Herrmann 1985; Herrmann and Kolb 1986). Hasmy et al. (1997) reported that there is a critical volume fraction for a system to gel and the gel time is system size dependent. This is in contradiction to the results of Gimel et al. (1995) and Rottereau et al. (2004). Heine and Pratsinis studied coagulation in a highly concentrated aerosol via Langevin dynamics calculations (Heine and Pratsinis 2006, 2007). They found that self-preserving distributions were obtained and the coagulation rate increased relative the dilute situation. They

did not study cluster morphology. Lushnikov (2005) did a theoretical study of the formation of a gel in a disperse system wherein binary coagulation alone governs the temporal changes in the particle size distribution. However, his study is based on the assumption that the aggregation kernel is proportional to the product of masses of aggregating particles, i.e., $K(v, u) = 2vu$, which is a case with homogeneity $\lambda = 2$. He also considered the SE to be valid throughout the aggregation process and reported on the exact solution of this model of non-Brownian kernel for a finite total mass of the coagulating system.

In this article we present experimental results of a study of aerosol fractal aggregate growth kinetics as the system evolved from cluster dilute to cluster dense and then gelled. Carbonaceous particle aerosols were created inside a closed optical chamber and their kinetics and morphology were studied using a small angle light scattering technique. We measured the kinetic exponent z, from which the kernel homogeneity, $\lambda$, was determined. We also measured the coagulation rate. We find that our experimental results are consistent with our simulations described above.

## THEORY

### The Aggregation Kernel

For the DLCA aggregation processes any two clusters can be treated like impenetrable spheres, with collision radii proportional to and roughly equal to their radii of gyration, following random trajectories before collision. Hence the aggregation kernel $K$ in the SE for DLCA is the Brownian kernel given as (Friedlander 2000; Seinfeld 1986),

$$K(v, u) = 4\pi(D_v + D_u)(R_v + R_u). \quad [4]$$

Here $R_v$ is the collision radius and $D_v$ is the Stokes-Einstein diffusion coefficient for clusters of size $v$. The diffusion coefficient $D$ is given as,

$$D = k_B T/6\pi\eta R_m \quad [5]$$

where $k_B$ is the Boltzmann's constant, $T$ the absolute temperature, $\eta$ the shear viscosity of the medium fluid, and $R_m$ the mobility radius of the diffusing cluster. With the use of Equations (3) and (5) in Equation (4), the Brownian kernel can be rewritten as,

$$K(v, u) = \frac{2k_B T}{3\eta}\left(v^{-1/D_f} + u^{-1/D_f}\right)\left(v^{1/D_f} + u^{1/D_f}\right). \quad [6]$$

For systems that are not cluster dilute an approach more general than that above is useful. A simple scaling argument can be used to determine limiting cases of the functional form of the kernel, and hence to determine the homogeneity (Pierce et al. 2006). The rate at which two particles collide, $K$, is proportional to their relative collision cross-sectional area $A_c$ and relative velocity $\dot{r}$. Thus we can write the aggregation kernel as $K \sim A_c\dot{r}$, consistent with the units of $[L^3/t]$. The relative collision cross-sectional area $A_c$ is the effective area seen by one cluster during its collision with another. Hence it is logical to write $A_c \sim R_g^2$. For the diffusing aggregate the relative velocity goes as $\dot{r} \sim D/R_c$, where $R_c$ is a characteristic length scale with respect to the given aggregate's motion. The diffusion constant goes as $D \sim 1/R_g$ in the case of the Stoke-Einstein diffusion. Thus $K \sim R_g/R_c$. Furthermore, for the cluster dilute situation $R_g$ is the only relevant length scale. Therefore, by default, $R_c \sim R_g$ and $K \sim 1$. Hence in the dilute limit continuum system with Stoke-Einstein diffusion (DLCA limit) $K$ has no size dependence resulting in $\lambda = 0$.

As the system continuously evolves, the available volume for the cluster to diffuse (free volume) decreases and hence the nearest neighbor cluster separation $R_{nn}$ eventually becomes a relevant length scale $R_c$ with respect to any given cluster's motion. We call this case the *intermediate* regime. For a system with an average cluster number density of $n_c$ at any time during aggregation process in $d$-dimensional space, the nearest neighbor cluster separation goes as $R_{nn} \sim n_c^{-1/d}$. The average cluster number density $n_c$ is related to the average monomer number density in the system $n_m$ and the average number of monomers $N$ in one single cluster as $n_c = n_m/N$. Since $n_m$ is a conserved quantity, $R_{nn}$ can equivalently be expressed in terms of the number of monomers in one cluster $N$ as $R_{nn} \sim N^{1/d}$. Thus at some intermediate time when the free volume is significantly less than the total volume, one can express the aggregation kernel $K$, considering the fact that $R_g \sim N^{1/D_f}$, as $K \sim N^{(\frac{1}{D_f} - \frac{1}{d})}$, which then gives

$$\lambda \sim \frac{1}{D_f} - \frac{1}{d} \quad [7]$$

Thus for the intermediate regime, with $D_f = 1.8$ and $d = 3$, Equation (8) yields $\lambda = 0.22$. This behavior has been seen in recent simulations (Pierce et al. 2006).

We remark that the intermediate regime is one in which $R_{nn}$ is no longer orders of magnitude greater than $R_g$ but still perhaps a factor of two to an order of magnitude greater than $R_g$. Thus $R_c = R_{nn}$, not the spacing between cluster surfaces. When $R_{nn}$ is yet smaller than say a factor of two times $R_g$, then the system enters the very dense regime described below.

For very dense systems, the aggregating particles start developing a connectivity network among themselves. Such systems are near the gel point. In this extreme, cluster dense limit, the distance between extended edges of the cluster become comparable to the persistence length, the distance over which a cluster moves effectively in a straight line. Thus the overall cluster motion between collisions is "ballistic-like." The cluster velocity is determined via the equipartition of energy as $\dot{r} \sim N^{-1/2}$. In such a crowded state, a cluster sees the "finger-like" detail of a neighbouring fractal aggregate and thus the relative collision

cross-sectional area $A_c$ must be replaced by the cluster's surface area $A_s$ in the scaling form of the aggregation kernel, hence from the scaling argument above $K \sim A_s \dot{r}$. Since all the monomeric particles in a fractal cluster are on the surface, the surface area of a cluster goes as the number of monomers in the cluster, i.e., $A_s \sim N$. Thus one finds that $K \sim N^{1/2}$ hence $\lambda = 0.5$ in the cluster dense regime.

## Aggregation Kinetics

The self-preserving scaling solution of the SE (Equation [1]) with homogeneous aggregation kernel in the asymptotic time limit has the form (Friedlander 2000; Friedlander and Wang 1966; Lai et al. 1972; Oh and Sorensen 1997);

$$n(v, t) = M_1 s_p^{-2} \phi(x) \qquad [8]$$

In Equation (8) $M_1$ is the first moment of the cluster size (mass or monomer number) distribution. In general the ith moment of the size distribution $M_i$ is given by

$$M_i(t) = \int_0^\infty v^i n(v, t)\, dv \qquad [9]$$

Also in Equation (8) $s_p = M_p/M_{p-1}$ is a time dependent $p^{\text{th}}$ order mean cluster size and $\phi(x)$ is the scaling function given by

$$\phi(x) = A x^{-\lambda} \exp(-\alpha x), \quad x \gg 1 \qquad [10]$$

where $x = v/s_p$ is the scaled cluster size, $A$ is a normalization constant and $\alpha = p - \lambda$ (Oh and Sorensen 1997).

Using Equation (8) in Equation (9) and substituting $x = v/s_p$ one finds

$$M_i(t) = M_1 s_p^{i-1} m_i \qquad [11]$$

where

$$m_i = \int_0^\infty x^i \phi(x) dx \qquad [12]$$

is the $i^{\text{th}}$ moment of the scaling function; $m_1 = 1$ by definition.

Use of Equation (10) in Equation (12) yields

$$m_i = A \alpha^{\lambda - i - 1} \Gamma(i + 1 - \lambda) \qquad [13]$$

where $\Gamma(x)$ is the Gamma function. The moments of the size distribution are found to obey the following relation when Equation (8) is substituted into the SE

$$M_i(t) = M_i(0)\,(1 + t/t_c)^{z(i-1)} \qquad [14]$$

where $t_c$ is a characteristic time depending on the aggregation kernel $K$, homogeneity $\lambda$, and the monomer number density $n_m$. Also, $z$ is the kinetic exponent related to the homogeneity $\lambda$ by

$$z = 1/(1 - \lambda). \qquad [15]$$

Hence for mean field aggregation the growth kinetics and the resulting size distribution are linked through the relation between $z$ and $\lambda$. Using the homogeneity at different regimes one can easily find $z \approx 1$, 1.28, and 2 for dilute limit continuum, intermediate and cluster crowded ballistic regimes, respectively.

In the Rayleigh light scattering limit the power scattered by a cluster of size $v$ goes as $v^2$. For this reason we choose $p = 2$ for $s_p$ (out of the infinite possible values) to interpret the light scattering studies. Thus the mean cluster size becomes $s_2 = M_2/M_1$. For the same reason in light scattering experiments one measures the second moment of the cluster size distribution, whose time derivative can be derived from the SE (Equation [1]) as

$$\frac{dM_2(t)}{dt} = \dot{M}_2(t) = \frac{1}{2} \int_0^\infty \int_0^\infty [(v + u)^2 - v^2 - u^2] K(v, u) n(v, t) n(u, t) dv du. \qquad [16]$$

Use of Equations (2) and (10) in Equation (16) and replacement of $v$ and $u$ by scaled cluster sizes $x$ and $y$, respectively, yields

$$\dot{M}_2(t) = s_2^\lambda M_1^2 I_2 \qquad [17]$$

where

$$I_2 = \frac{1}{2} \int_0^\infty \int_0^\infty [(x + y)^2 - x^2 - y^2] K(x, y) \phi(x) \phi(y) dx dy. \qquad [18]$$

Equation (17) can be modified by multiplying it with $s_2^{-\lambda} K(s_2, s_2)/K(1, 1) = 1$ since $K$ is a homogeneous function (Equation [2]). This yields

$$\dot{M}_2(t) = M_1^2 P_2 K(s_2, s_2) \qquad [19]$$

where

$$P_2 = I_2/K(1, 1) \qquad [20]$$

is the polydispersity index; $P_2 = 1$ for a monodispersed system.

The mean cluster size $s_2$ and the first moment of the cluster size distribution $M_1$ (total mass or monomer number density) can give a measure of the average cluster number density as $n_2 (= n_c) = M_1/s_2 = M_1^2/M_2$. Its time derivative using Equation (19) is given by

$$\dot{n_2} = -\left({M_1}^2/M_2^2\right) \dot{M}_2 = -n_2^2 P_2 K(s_2, s_2). \qquad [21]$$

Thus

$$K(s_2, s_2) = P_2^{-1} \frac{d}{dt}\left(\frac{1}{n_2}\right). \quad [22]$$

In our light scattering experiment we measure $n_2$. Then the kernel $K(s_2, s_2)$ is determined from the slope of the plot of $n_2$ versus time using Equation (22). We have used $P_2 = 1.10$ as the polydispersity index determined numerically for DLCA (Oh and Sorensen 1997). The following section gives the theoretical background on the light scattering technique in greater detail.

## Light Scattering

Light scattering is an extremely useful non-perturbative technique that can yield real time size and fractal dimension information for an aggregating system. The intensity scattered by an aggregate normalized by the forward scattered intensity gives the measure of its structure factor $S(q)$ (Sorensen 2001). The variable $q$ is the scattering wave vector at scattering angle $\theta$ given by

$$q = 4\pi\lambda^{-1}\sin(\theta/2). \quad [23]$$

The effective structure factor for an ensemble of polydispersed, RDG aggregates can be written as (Sorensen 2001)

$$S_{eff}(q) \approx 1, \qquad qR_{gz} \ll 1 \quad [24a]$$

$$S_{eff}(q) \approx 1 - \frac{1}{3}q^2R_{gz}^2, \qquad qR_{gz} \leq 1 \quad [24b]$$

$$S_{eff}(q) = CC_p\left(qR_{gz}\right)^{-D_f}, \; qR_{gz} \gg 1. \quad [24c]$$

In Equation (24) $R_{gz}$ is the so-called z-average radius of gyration which represents the size averaged over the distribution weighted by the light scattering cross-section hence the square of the cluster mass. The z-average radius of gyration $R_{gz}$ is given by

$$R_{gz}^2 = a^2k_0^{-2/D_f}s_2^{2/D_f}m_{2+2/D_f}/m_2. \quad [25]$$

Also in Equation (24c), $C$ is a proportionality constant of order of unity, and $C_p$ is the polydispersity factor of the ensemble given by (Sorensen 2001)

$$C_p = \frac{M_1}{M_2}\left(\frac{M_{2+2/D_f}}{M_2}\right)^{D_f/2}. \quad [26]$$

Equation (24) have been derived under the assumption of the Rayleigh-Debye-Gans (RDG) approximation which considers a scatterer as a set of independent, non-interacting Rayleigh scattering elements (Sorensen 2001), i.e., no internal (i.e., within a single scattering cluster) multiple scattering. The veracity of these equations has been established both experimentally (Cai et al. 1993; Wang and Sorensen 2002) and computationally (Farias 1996).

One needs to be careful here to see the difference between the z-average radius of gyration $R_{gz}$ and the radius of gyration $R_{g2}$ of the average cluster size $\langle N\rangle = s_2$. It follows from Equation (3) that the mean sized cluster radius of gyration is

$$R_{g2} = ak_0^{-1/D_f}s_2^{1/D_f}. \quad [27]$$

Equations (25) and (27) can be combined to relate $R_{gz}$ and $R_{g2}$ as

$$R_{gz}^2 = R_{g2}^2(m_{2+2/D_f}/m_2). \quad [28]$$

The time dependence of either $R_g$ is due to $s_2$ which for long time goes as $t^z$. Thus

$$R_g \sim t^{z/D_f}. \quad [29]$$

Equation (25) can be rewritten for the average cluster number density $n_2 = M_1/s_2$, using the fact that $M_1 = f_v/(4\pi a^3/3)$, as

$$n_2 = \frac{3f_v}{4\pi k_0 a^{3-D_f}R_{gz}^{D_f}}\left(\frac{m_{2+2/D_f}}{m_2}\right)^{D_f/2}. \quad [30]$$

$R_{gz}$ in Equation (30) is directly measured from light scattering experiments while transmission electron microscopy gives $a$. Hence the cluster number density can be evaluated once the size distribution and the monomer volume fraction are known. The aggregation kernel $K(s_2, s_2)$ can then be determined from the rate at which $1/n_2$ grows with time according to Equation (22).

The monomer volume fraction $f_v$ in Equation (30) can be determined by measuring the absorption coefficient $\tau_{abs}$ of the system and then using the relation

$$f_v = \tau_{abs}/3kE(m) \quad [31]$$

where $k = 2\pi/\lambda$ is the wave number of the incident laser beam, $E(m) = \mathrm{Im}[(m^2-1)/(m^2+2)]$ where "Im" means the imaginary part and $m$ is the monomer refractive index. Determination of $\tau_{abs}$ is not straightforward since a turbidity measurement yields the extinction coefficient $\tau_{ext}$ which is the sum of both scattering ($\tau_{scat}$) and absorption ($\tau_{abs}$) coefficients. However we can extract $\tau_{abs}$ from $\tau_{ext}$ if we know the albedo $\omega = \tau_{scat}/\tau_{ext}$ of the system. $\tau_{ext}$ is determined by measuring both the incident $I_0$ and transmitted $I_T$ intensities and using Beer's law

$$I_T = I_0\exp(-\tau_{ext}l). \quad [32]$$

Here $l$ is the optical path length of the beam through the system. The albedo $\omega$ relates $\tau_{ext}$ and $\tau_{abs}$ as

$$\tau_{abs} = \tau_{ext}(1 - \omega). \quad [33]$$

The albedo $\omega$ for a system of aggregates depends on the refractive index of the monomeric particle, the incident wavelength, the fractal dimension and the radius of gyration of the aggregates and is given by the relation (Sorensen 2001)

$$\omega = \left[1 + \frac{3}{2}\frac{E(m)}{F(m)}\frac{1}{k_0}(ka)^{D_f-3}\left(\frac{1}{k^2R_g^2} + \frac{4}{3D_f}\right)^{D_f/2}\right]^{-1} \quad [34]$$

where $F(m) = |(m^2 - 1)/(m^2 + 2)|^2$.

With the theoretical background described here, we performed light scattering experiments with aggregating carbon soot particles. The different monomer volume fractions $f_v$ were achieved by varying the amount of hydrocarbon in the gaseous mixture inside the chamber. We observed the time evolution of the kinetics and morphology of the aggregating clusters with different monomer volume fractions. The experimental details, results and discussions are what follow.

## EXPERIMENTS

Carbonaceous soot aerosols were created by exploding a mixture of acetylene ($C_2H_2$) and oxygen filled in a closed, cylindrical disk combustion chamber with circular glass windows on both ends of the cylinder. The small gas volume quickly cools. After the explosion the pressure is about 30% larger than atmospheric pressure so we can estimate the gas molecule mean free path to be about 50 nm. This is comparable to the soot monomer size (ca. 38 nm, see below) so the system starts aggregating in the transition regime (Friedlander 2000). In a few seconds, however, the aggregates grow to 300 nm where our light scattering apparatus can begin viable measurements. Thus for our studies here the system is in the continuum limit. The internal space of the chamber was 51 mm diameter wide and 10 mm thick. The monomer volume fraction $f_v$ could be controlled by the amount of gas mixture in the chamber prior to the explosion.

We used a Small Angle Static Light Scattering (SASLS) technique (Ferri 1997) to study the morphology and kinetics of the quickly aggregating carbon soot particles after they were rapidly produced during the explosion. This technique involves measurement of the scattered light intensity $I(q)$ as a function of the scattering wave vector $q$ over a horizontal scattering plane. An unfocused, vertically polarized argon ion laser beam with a 1.0 mm beam waist operating at wavelength $\lambda = 488$ nm entered normally into the optical chamber through one of its glass windows. Since the aggregates can grow bigger than 10 $\mu$m in size, which corresponds to small $q$, the measurements were confined to a range of small scattering angles $0.1^\circ \leq \theta \leq 15^\circ$ over a horizontal scattering plane, which corresponds to $q$ values in the range 200 $cm^{-1} \leq q \leq 3 \times 10^4$ $cm^{-1}$. The scattered light along with unscattered beam left the chamber through the other glass window. A first lens collected the light scattered at constant angle and focused this at its Fourier plane. The unscattered beam was removed using a tiny mirror at the axial focus on the Fourier plane. A second lens imaged the Fourier plane onto a horizontal photodiode array. The detector was interfaced with a computer, which handled and recorded the acquired data. The SASLS device was calibrated by diffracting the laser beam through a 10 $\mu$m single slit and also by scattering the beam from 9.6 $\mu$m polystyrene colloidal particles.

A time series light scattering data for the whole range of scattering angles measured by the photodetector array were recorded by the computer starting right after the explosion in the chamber until the system gelled. After gelation, there was no more evolution in the scattering pattern. The scattered intensity data were recorded for different runs with different monomer volume fraction $f_v$.

The monomer volume fraction $f_v$ of the aggregating system was determined via extinction measurements and application of Equations (31) to (34). For the extinction measurement the attenuated incident beam was focused and passed through a small aperture stop to eliminate forward scattered light. The monomer size $a$ of the soot aggregates was directly measured from transmission electron microscope (TEM) pictures.

## RESULTS AND DISCUSSION

Immediately after the aerosol was created in the explosion, the scattered light intensity pattern was found to evolve and then stop about 30 to 100 s later depending upon the monomer volume fraction $f_v$. The system evolved faster with higher $f_v$ and gelled whenever $f_v \geq 1.0 \times 10^{-4}$. This implies that the clusters grew from the monomer size of ca. 38 nm to $\geq$10 microns at the gel point. Visual inspection showed that the gel spanned the volume of the scattering chamber.

### Monomer Volume Fraction Measurement

Extinction measurements can yield the aggregate monomer volume fraction $f_v$ if the refractive index of the material has an imaginary part. Soot has a complex refractive index, but it is poorly known. Many soot refractive index measurements exist in the literature, and there is little reason to choose one measurement as the best (Sorensen 2001) although Bond and Bergstrom (2006) have recently brought some order to this problem.

In our analysis we pick reasonable E(m) and E(m)/F(m) values which can be surmised from the great varieties of refractive indices rather that pick a specific value of m. The volume fraction $f_v$ is related to E(m) as shown in Equation (31). The values of $E(m)$ corresponding to the soot refractive indices found in the literature are found to lie in the range 0.19–0.37. Here we chose $E(m) = 0.26$, a typical value for a soot system. It also appears in the albedo (Equation [34]) via the factor $3(E/F)/2k_{\circ}$.

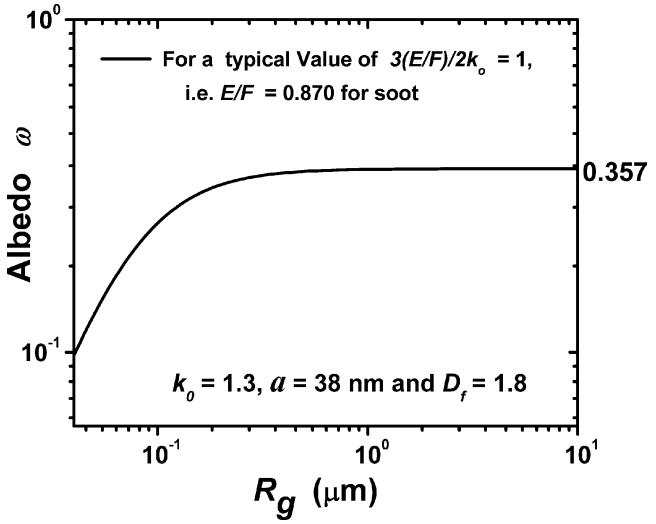


FIG. 1. A graph of albedo $\omega$ (Equation [34]) against the cluster radius of gyration $R_g$ with $3(E/F)/2k_\circ = 1$, a typical value for soot fractal aggregates, and $\lambda = 488$ nm. Here we used the carbon soot monomer size (radius) $a = 38$ nm as shown by TEM pictures, and the fractal dimension $D_f = 1.8$.

A typical value of this factor for soot fractal aggregates is equal to 1 (Sorensen 2001). This implies $E/F = 0.87$ if $k_\circ = 1.3$. Figure 1 shows a plot of the albedo $\omega$ versus the aggregate size $R_g$, Equation (34), for our experimental scattering wavelength ($\lambda = 488$ nm) with $3(E/F)/2k_\circ = 1$, and indicates $\omega \approx 0.357$ in the experimentally measured range of $R_g$. Here we used the carbon soot monomer size (radius) $a = 38$ nm as shown by TEM pictures, and the fractal dimension $D_f = 1.8$ (the widely accepted value for DLCA clusters). Following the uncertainty in the ratio $E/F$ due to the uncertainty in the soot refractive index, we find $\omega = 0.357 \pm 0.090$ for the soot clusters with $R_g > 1$ $\mu$m. Using this value of $\omega$, the absorption coefficient $\tau_{abs}$ was extracted from the extinction coefficient $\tau_{ext}$ determined from experimental data using Beer's law (Equation [32]), and hence $f_v$ was measured using Equation (31) and accounting for the error in $E(m)$. Bond and Bergstrom (2006) suggest $\omega = 0.25 \pm 0.05$ which overlaps our value. Use of this value would increase $f_v$ by 17%.

## Interpretation of Light Scattering Data with Multiple Scattering Effects

Under the RDG assumption, the fractal dimension of the evolving aggregates is the magnitude of the slope with which $I(q)$ decreases with increasing $q$ after the initial flat Rayleigh regime on a log-log plot, see Equation (24c). However, inter-cluster multiple scattering can hinder this analysis. Multiple scattering tends to illuminate the whole scattering angular range uniformly, hence will give an apparent fractal dimension too low. To test for the presence of multiple scattering and to decrease its effects we measured and analysed the scattered intensities $I(q)$ from the aggregating soot system with different optical path lengths at a given volume fraction $f_v$. It has been established that the extent of multiple scattering is proportional to the viewed optical path length (Mokhtari et al. 2005). We decreased the optical path length by gluing a small extra glass piece, a disk with diameter 0.63 inch, between the two windows of the optical chamber and thereby decreasing the optical path length in a small portion of the chamber. Figures 2a, 2b, and 2c show the plot of $I(q)$ versus $q$, evolving with time, with the optical path lengths 10 mm, 3 mm, and 1.5 mm, respectively, keeping the proportion of acetylene and oxygen and the amount of the mixture the same.

As is clear from these figures, the magnitude of the slope (apparent $D_f$ ) increased from 1.4 to 1.6 as the optical path length decreased from 10 mm to 1.5 mm. We interpret this as a consequence of decreased multiple scattering at small optical path lengths. Our TEM image analyses of the soot clusters at monomer length scales had however showed that $D_f \approx 1.8$, the DLCA value. The implication was that the expected $D_f = 1.8$ probably would have been revealed if we could further decrease the optical path length below 1.5 mm. Our attempts to scatter light from the system with optical path length lower than 1.5 mm failed since no soot formed in the very thin region during the gas mixture explosion. Hence we confined all our experiments to 1.5 mm optical path length (note that this is still large compared to the biggest cluster sizes of ca. 0.01 mm). The multiple scattering effects were also found to grow stronger when the monomer volume fraction $f_v$ was increased above $8 \times 10^{-5}$. The apparent fractal dimension hence further decreased below 1.6. We thus need to pay extra attention while determining fractal dimension from light scattering data.

## Kinetic Exponent z (and Homogeneity λ) Measurements

We measured the time evolving cluster sizes $R_{gz}$, i.e., z-averaged radii of gyration, by a Guinier analysis (Sorensen 2001) of the scattered intensity using Equation (24b). We found $R_{gz}$ to increase up to about 10 $\mu$m or a little higher by the time the system stopped evolving at the gel point. The slope of a log-log plot of $R_{gz}$ against time $t$ gives the ratio of the kinetic exponent $z$ and the fractal dimension $D_f$ according to the power-law $R_g \sim t^{z/D_f}$, Equation (29). Thus with known $D_f$, $z$ and hence the homogeneity $\lambda$ (Equation [15]) can be determined. Here we assume that the mean field relation Equation (15) holds at all time during the aggregation process and for all volume fraction, $f_v$, an assumption substantiated by our simulation study (Fry et al. 2002, 2004).

Figure 3 illustrates a typical example of $R_{gz}$ evolving with time, in log-log scale, for an aggregating system with $f_v \approx 5.1 \times 10^{-5}$. We used the DLCA value of fractal dimension, i.e., $D_f = 1.8$, to determine $z$ (and hence $\lambda$) from the slope with which $R_{gz}$ evolved with time. Figure 4 shows the average (over several runs with the same monomer volume fraction) values of kinetic exponent z and the homogeneity $\lambda$ at different monomer volume fractions $f_v$. At lower $f_v$ we found $z \approx 1$ (and $\lambda \approx 0$) consistent with the cluster dilute, DLCA case. With increasing

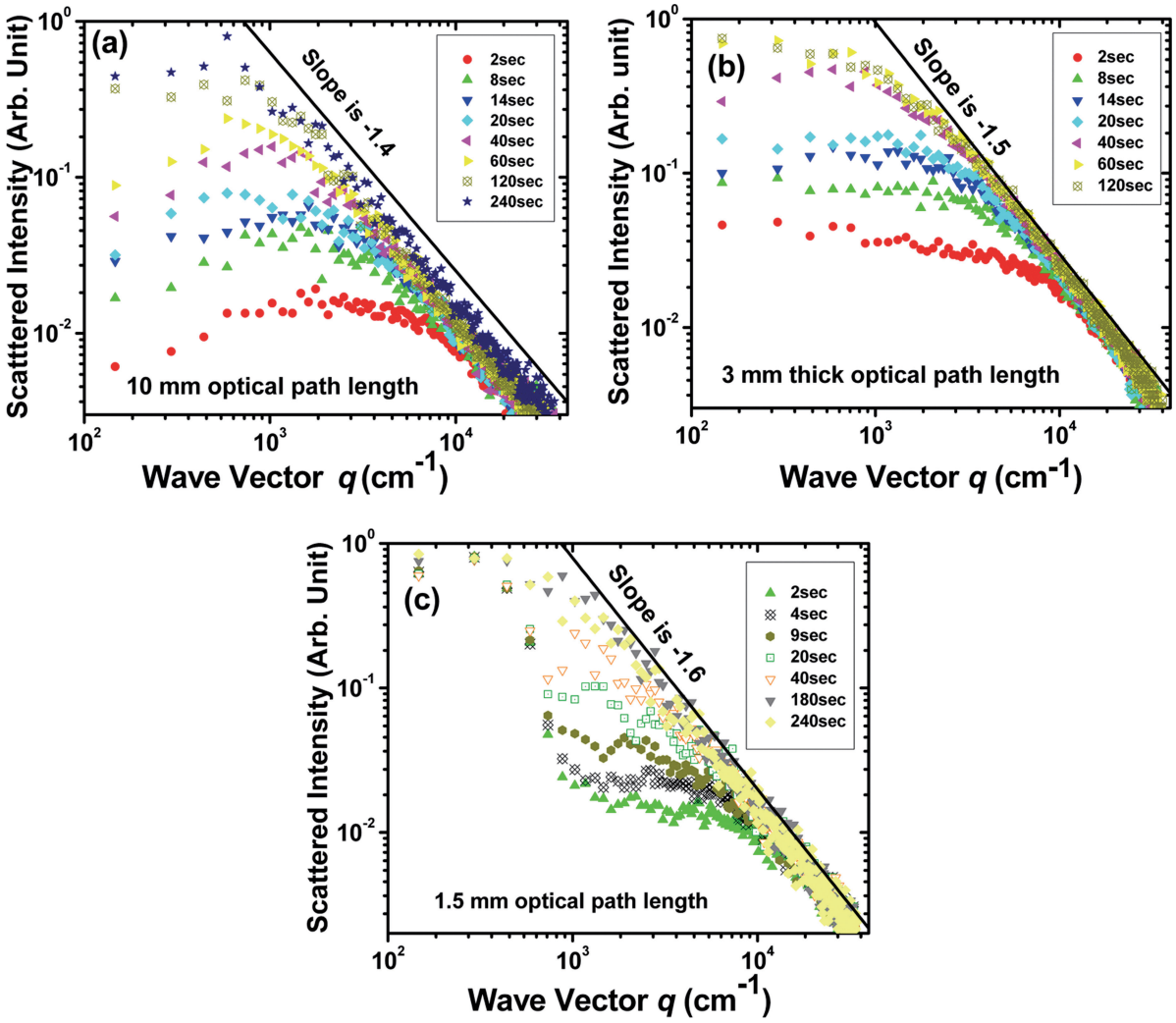


FIG. 2. Log-log plot of scattered intensity versus the scattering wave vector $q$ evolving with time when the optical path length for the laser beam through the scattering volume is (a) 10 mm, (b) 3 mm, and (c) 1.5 mm. The time elapsed when a measurement was taken after the creation of the aerosol is indicated. The system stops evolving when the gel point is reached after about 120 s. The effect of multiple scattering becomes larger with increasing optical path length as indicated by a smaller apparent fractal dimension.



monomer volume fraction $f_v$, $z$ (and $\lambda$) was also found to increase up to 1.9 (and $\lambda$ up to 0.4) indicating the enhanced aggregation kinetics functionality. This increasing value of $z$ (and $\lambda$) is consistent with our simulation results (Fry et al. 2002, 2004) indicating the transition of the aggregating system from the cluster dilute to the cluster dense limit, as discussed in the theory section of this article. The enhanced aggregation kinetics was the result of the effect of cluster crowding which creates less free volume in which to search for other clusters for the diffusing clusters.

Enhanced kinetics has also been reported by Carpineti et al. (1990), without explanation, at later times during the salt induced aggregation of 130 nm diameter polystyrene colloidal particles. They found faster growth to occur earlier in time when monomer concentration was increased. Reworking their data we found the kinetic exponent $z$ to increase from 1.3 to 2.3 after the onset of enhanced kinetics for $1 \times 10^9$ monomer concentration. We propose that this enhanced kinetics was the result of the transition of the system from cluster dilute to cluster dense regime.

We expect all aggregating systems starting from the cluster dilute regime to enter the cluster dense regime eventually. However, for systems with small monomer volume fraction $f_v$, the aggregation time scales were slower than the gravitational settling time scale so that gravitational settling overwhelmed the aggregation process. This limited our experiments to systems with volume fractions greater than ca. $10^{-5}$. On the other hand for the systems with $f_v > 10^{-4}$, the transition from cluster-dilute to cluster-dense was so fast (less than few seconds and gelation in 30 s) that we had difficulty in resolving the

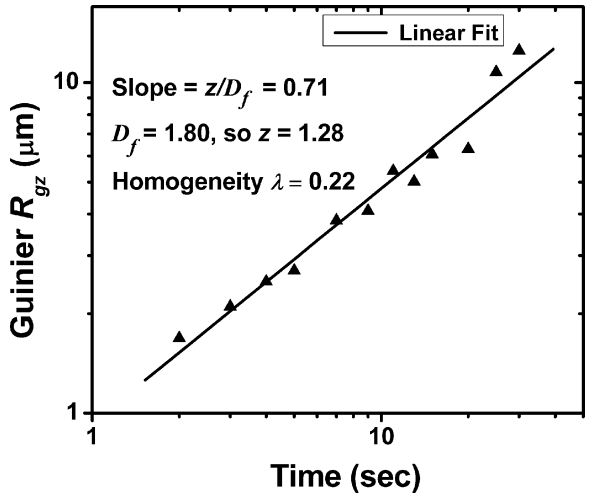


FIG. 3. Growth of cluster radius of gyration with time when $f_v = 5.1 \times 10^{-5}$. The cluster radius of gyration is determined using Guinier analysis of the scattered intensity data.

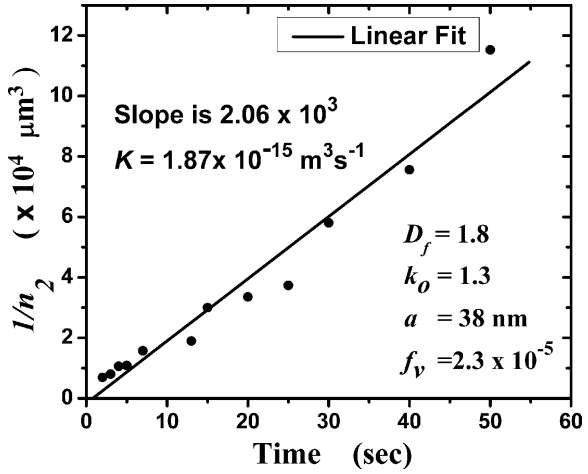


FIG. 5. An example of the plot of the inverse cluster number density $1/n_2$ versus time $t$ when $f_v = 2.3 \times 10^{-5}$.

kinetics. Thus our experiments were constrained between these limits.

### Aggregation Kernel *K*

To obtain the aggregation kernel we first determined the cluster number density $n_2$ using Equation (30). Here we used $D_f = 1.8$, $a = 38$ nm (as measured from TEM image), $\lambda = 0$, $k_\circ = 1.3$ and the volume fraction determined via extinction measurements, Equations (31) to (34). Figure 5 shows a typical example of the plot of the inverse cluster number density $1/n_2$ versus time $t$. The slope of this curve divided by the polydispersity index $P_2$ gives the value of aggregation kernel $K(s_2, s_2)$ for equal sized clusters in accordance with Equation (22). We used $P_2 = 1.10$ as determined numerically for DLCA (Lai et al. 1972).

The values of $K(s_2, s_2)$ we determined are the average over the entire period from monomers to the gel. Most of our plots like Figure 5 showed an upward curvature to imply that the rate was increasing during the run. This is consistent with theoretical expectation. We did not quantify this, however, because the curvature effect was the same size as our experimental error. We also ignored the variation in the homogeneity λ because increasing λ from 0 (for dilute system) to 0.5 (dense system) introduced only ∼10% change in the cluster number density measurement, and owing to the uncertainty in the monomer volume fraction $f_v$ measurements this ∼10% change was within the uncertainty limit.

Figure 6 gives the average (over several runs with the same monomer volume fraction) values of $K(s_2, s_2)$ as a function of the monomer volume fraction $f_v$ for our carbon soot system. The values of $K(s_2, s_2)$ lie in the range $1.5 \times 10^{-15}$ to $5.0 \times 10^{-15}$ m$^3$/sec and increase slightly with $f_v$. This indicates the speeding up of aggregation kinetics as $f_v$ was increased. This result is strongly influenced by the soot refractive index value chosen from a broad range of values available in the literature. The uncertainty $\Delta K$ in $K(s_2, s_2)$ can be obtained from Equations (22), (30), (31), and (33) as

$$\frac{\Delta K}{\bar{K}(s_2, s_2)} = \frac{\Delta\omega}{(1-\bar{\omega})} + \frac{\Delta E(m)}{\bar{E}(m)}. \qquad [35]$$

Here $\bar{K}, \bar{\omega}$, and $\bar{E}$ are the respective averages. Since the reported values of $E(m)$ corresponding to the soot refractive indices lie in the range 0.19–0.37, we assumed $\bar{E}(m) = 0.260$ and $\Delta E(m) = 0.080$. Also we took $\bar{\omega} = 0.357$ and $\Delta\omega = 0.090$. Then Equation (35) predicts an uncertainty of $\Delta K/K(s_2, s_2) \sim 45\%$. Despite this uncertainly, our conclusion about the qualitatively

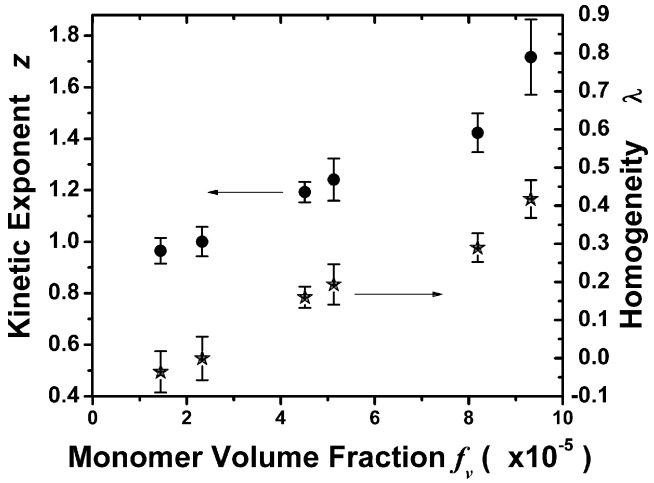


FIG. 4. A plot of the average kinetic exponent $z$ and the homogeneity λ versus the monomer volume fraction $f_v$. The vertical bars represent the errors introduced while determining $z$ and λ. The enhanced aggregation kinetics with increasing $f_v$ was the result of the effect of cluster crowding.

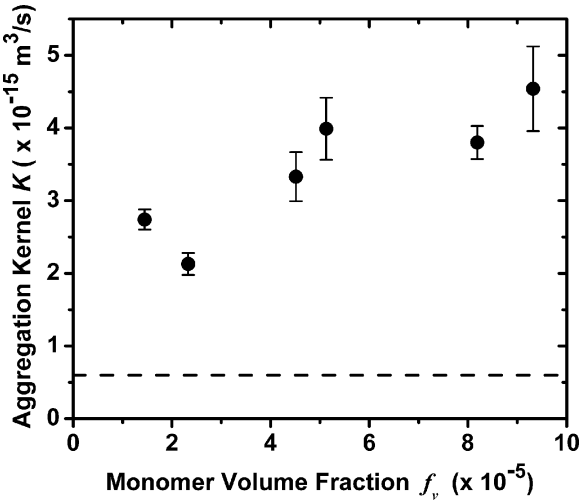


FIG. 6. A plot of the average $K(s_2, s_2)$ as a function of the monomer volume fraction $f_v$. The vertical bars represent the errors introduced in $K(s_2, s_2)$ while determining the rate of change of $1/n_2$ with time $t$, and not the uncertainty due to the uncertain index of refraction of soot. The dashed line shows the theoretical value of $K$ independent of the monomer volume fraction. The theoretical $K$ was computed for a monodispersed aggregating system in continuum regime with Stokes-Einstein diffusion.

increasing trend in the values of $K(s_2, s_2)$ with volume fraction is still reliable.

Figure 6 also shows the comparison of $K(s_2, s_2)$ with the theoretical value (Equation [6]) for a monodispersed system in the cluster dilute, continuum regime aggregating with Stokes-Einstein diffusion. The theoretical $K$ is independent of the monomer volume fraction. The measured values of $K(s_2, s_2)$ were found to be larger by a factor of 3.5 or more. This is consistent with our previous simulations for aggregation in the cluster dense regime (Fry et al. 2002, 2004).

## CONCLUSIONS

By employing the SASLS technique we investigated the aggregation kinetics of a dense aggregating aerosol system at different monomer volume fractions. We found $z \approx 1$ (and $\lambda \approx 0$) consistent with the cluster dilute, DLCA case at lower monomer volume fractions $f_v$. With increasing monomer volume fraction $f_v$, $z$ (and $\lambda$) was found to increase up to 1.7 +/– 0.14 (and $\lambda$ up to 0.42 +/– 0.05) indicating enhanced aggregation kinetics functionality. This result is consistent with simulation results from our laboratory (Fry et al. 2002, 2004) indicating the transition of the aggregating system from the cluster dilute to the cluster dense limit. We also found the measured rates of aggregation, $K(s_2, s_2)$, lie in the range $1.5 \times 10^{-15}$ to $5.0 \times 10^{-15}$ m$^3$/s which is faster than the dilute limit value. These rates increased slightly with $f_v$ which is also consistent with simulations (Fry et al. 2002, 2004).

## REFERENCES


Bond, T., and Bergstrom, R. (2006). Light Absorption by Carbonaceous Particles: An Investigative Review, *Aerosol Sci. Technol*. 40:27–67.

Cai, J., Lu, N., and Sorensen, C. S. (1993). Comparison of Size and Morphology of Soot Aggregates as Determined by Light Scattering and Electron Microscope Analysis, *Langmuir* 9:2861–2867.

Cai, J., Lu, N. L., and Sorensen, C. M. (1995). Analysis of Fractal Cluster Morphology Parameters: Structural Coefficient and Density Autocorrelation Function Cutoff, *J. Colloid Interface Sci*. 171:470–473.

Carpineti, M., Ferri, F., Giglio, M., Paganini, E., and Perini, U. (1990). Salt Induced Fast Aggregation of Polystyrene Latex, *Phys. Rev. A* 42:7347–7354.

Chakrabarti, A., Fry, D., and Sorensen, C. M. (2004). Molecular Dynamics Simulations of the Transition from Dispersed to Solid Phase, *Phys. Rev. E* 69:031408–11.

Dhaubhadel, R., Pierce, F., Chakrabarti A., and Sorensen, C. M. (2006). Hybrid Superaggregate Morphology as a Result of Aggregation in a Cluster-Dense Aerosol, *Phys. Rev. E* 73:011404–4.

Dhaubhadel, R., Gerving, C., Chakrabarti, A., and Sorensen, C. M. (2007). Aerosol Gelation: Synthesis of a Novel Lightweight, High Specific Surface Area-Material, *Aerosol Sci. Tech.* 41:804–810.

Family, F., and Landau, D. P. (eds.). (1984). *Kinetics of Aggregation and Gelation*, North Holland, Amsterdam.

Farias, T. L., Koylu, U. O., and Carvalho, M. G. (1996). Range of Validity of the Rayleigh-Debye-Gans Theory for Optics of Fractal Aggregates, *Appl. Opt*. 35:6560–6567.

Ferri, F. (1997). Use of a Charge Coupled Device Camera for Low-Angle Elastic Light Scattering, *Rev. Sci. Instrum.* 68:2265–2274.

Friedlander, S. K., and Wang, C. S. (1966). The Self-Preserving Particle Size Distribution for Coagulation by Brownian Motion, *J. Colloid Interface Sci*. 22:126–132.

Friedlander, S. K. (2000). *Smoke, Dust and Haze*, Oxford University Press, New York.

Fry, D., Sintes, T., Chakrabarti, A., and Sorensen, C. M. (2002). Enhanced Kinetics and Free-Volume Universality in Dense Aggregating Systems, *Phys. Rev. Lett*. 89:148301–4.

Fry, D., Chakrabarti, A., Kim, W., and Sorensen, C. M. (2004). Structural Crossover in Dense Irreversibly Aggregating Particulate Systems, *Phys. Rev. E* 69:061401–10.

Gimel, J. C., Durand, D., and Nicolai, T. (1995). Transition between Flocculation and Percolation of a Diffusion-Limited Cluster-Cluster Aggregation Process using Three-Dimension Monte Carlo Simulation, *Physical Review B* 51:11348–58.

Hasmy A., and Jullien, R. (1996). Percolation in Cluster-Cluster Aggregation Processes, *Physical Review E* 53:1789–1794.

Hasmy, A., Anglaret, E., Thouy, R., and Jullien, R. (1997). Fluctuating Bond Aggregation: a Numerical Simulation of Neutrally-Reacted Silica Gels, *Journal De Physique* I 7:521–542.

Heine, M. C., and Pratsinis, S. E. (2006). High Concentration Agglomerate Dynamics at High Temperatures, *Langmuir* 22:10238–10245.

Heine, M. C., and Pratsinis, S. E. (2007). Brownian Coagulation at High Concentration, *Langmuir* 23:9882–9890.

Herrmann, H. J., and Kolb, M. (1986). Irreversible Aggregation of Clusters at High Density, *J. Physics A—Mathematical and General* 19:L1027–L1031.

Jullien, R., and Botet, R. (1987). *Aggregation and Fractal Aggregates.* World Scientific Publication, Hackensack, NJ.

Kim, W., Sorensen, C. M., and Chakrabarti, A. (2004). Universal Occurrence of Soot Superaggregates with a Fractal Dimension of 2.6 in Heavily Sooting Laminar Diffuion Flames, *Langmuir* 20:3969–3973.

Kim, W., Sorensen, C. M., Fry, D., and Chakrabarti, A. (2006). Soot Aggregates, Superaggregates and Gel-Like Networks in Laminar Diffusion Flames, *J. Aerosol Sci*. 37:386–401.

Kolb, M., Botet, R., and Jullien, R. (1983). Scaling of Kinetically Growing Clusters, *Phys. Rev. Lett*. 51:1123–1126.

Kolb M., and Herrmann, H. J. (1985). The Sol-Gel Transition Modelled by Irreversible Aggregation of Clusters, *J. Physics A—Mathematical and General* 18:L435.

Lai, F. S., Friedlander, S. K., Pich, J., and Hidy, G. M. (1972). The Self-Preserving Particle Size Distribution for Brownian Coagulation in the Free-Molecule Regime, *J. Colloid Interface Sci.* 39:395–405.

Lin, X. M., Jaeger, H. M., Sorensen, C. M., and Klabunde, K. J. (2001). Formation of Long-Range-Ordered Nanocrystal Superlattices on Silicon Nitride Substrates, *J. Phys. Chem. B* 105:3353–3357.

Lushnikov, A. A. (2005). Exact Kinetics of the Sol-Gel Transition, *Phys. Rev. E* 71:046129–10.

Meakin, P. (1983). Formation of Fractal Clusters and Networks by Irreversible Diffusion-Limited Aggregation, *Phys. Rev. Lett*. 51:1119–1122.

Meakin, P. (1988). Fractal Aggregates, *Adv. Colloid Interface Sci*. 28:249–331.

Meakin, P. (1992). Aggregation Kinetics, *Phys. Scripta* 46:295–331.

Meakin, P. (1999). A Historical Introduction to Computer Models for Fractal Aggregates, *J. Sol. Gel. Sci. Technol.* 15:97.

Mokhtari, T., Sorensen, C. M., and Chakrabarti, A. (2005). Multiple-Scattering Effects on Statistic Light-Scattering Optical Structure Factor Measurements, *Appl. Opt.* 44:7858.

Murray, C. B., Kagan, C. R., and Bawendi, M. G. (1995). Self-Organization of CdSe Nanocrystallites into Three-Dimensional Quantum Dot Superlattices, *Sci.* 270:1335–1338.

Oh, C., and Sorensen, C. M. (1997). Light Scattering Study of Fractal Cluster Aggregation Near the Free Molecular Regime, *J. Aerosol Sci*. 28:937–957.

Pierce, F., Sorensen, C. M., and Chakrabarti, A. (2006). Computer Simulation of Diffusion-Limited Cluster-Cluster Aggregation with an Epstein Drag Force, *Phys. Rev. E* 74:021411–8.

Rottereau, M., Gimel, J. C., Nicolai, T., and Durand, D. (2004). Monte Carol Simulation of Particle Aggregation and Gelation I. Growth, Structure and Size Distribution of the Clusters, *European Physical Journal E* 15:133–140.

Seaton, N. A., and Glandt, E. D. (1987). Percolation and Conduction in Colloidal Dispersions, *Physicochemical Hydrodynamics* 9:369.

Seinfeld, J. H. (1986). *Atmospheric Chemistry and Physics of Air Pollution*. Wiley, New York.

Smoluchowski, M. V. (1917). Mathematical Theory of the Kinetics of the Coagulation of Colloidal Solutions, *Z. Phys. Chem.* 92:129.

Sorensen, C. M., Hageman, W. B., Rush, T. J., Huang, H., and Oh, C. (1998). Aerogelation in a Flame Soot Aerosol, *Phys. Rev. Lett.* 80:1782–1785.

Sorensen, C. M., and Hageman, W. B. (2001). Two-Dimensional Soot, *Langmuir* 17:5431–5434.

Sorensen, C. M., and Roberts, G. C. (1997). The Prefactor of Fractal Aggregates, *J. Colloid Interface Sci*. 186:447–452.

Sorensen, C. M. (2001). Light Scattering from Fractal Aggregates: A Review, *Aerosol Sci. Technol.* 35:648–687.

Sorensen, C. M., Kim, W., Fry, D., Shi, D., and Chakrabarti, A. (2003). Observation of Soot Superaggregates with a Fractal Dimension of 2.6 in Langmuir Acetylene/Air Diffusion Flames, *Langmuir* 19:7560–7563.

Vicsek, T. (1989). *Fractal Growth Phenomena*. World Scientific, Singapore.

Wang, G., and Sorensen, C. M. (2002). Experimental Test of the Rayleigh-Debye-Gans Theory for Light Scattering by Fractal Aggregate*s, Appl. Opt*. 41:4645–4651.